Complex Permittivity Measurements of KAT-7 and MeerKAT Karoo Soil

Dr. Braam Otto

November 29, 2010

Abstract

To avoid saturating the extremely sensitive receivers used in radio telescopes they need to be situated in a radio quiet zone. The levels of unwanted signal attenuation by burying cables and bunkers containing “noisy" electronic equipment are investigated. The soil would not only help attenuate these noisy signals, but also give a level of protection to the equipment from interference from radiative outside noise like lightning. This is investigated by measuring the attenuation of induced signals on cables buried at various depths under ground. The complex permittivity of a soil sample taken from the core-site is furthermore determined using the iterative Baker-Jarvis extraction method. It is important to know the complex permittivity values of surrounding soil at the radio telescope sites in order to use the most accurate values in computational models of the dishes and their lightning protection systems. Good correlation between analytically predicted, numerically computed and site- as well as laboratory-measured attenuation results for the Karoo soil are found.

Acknowledgements

The author would like to acknowledge SKA South Africa, especially Dr. Richard Lord and Mr. Carel van der Merwe for their assistance in arranging the experimental setup in the Karoo; his postdoctoral supervisor Prof. Howard Reader; Mr. Renier Marchand for the assistance with the Baker-Jarvis extraction codes; Dr. Paul van der Merwe and Dr. Gideon Wiid for the assistance with measurements on site and in the laboratory.

The research was funded by SKA South Africa, the NRF and the University of Stellenbosch.

Contents

List of Figures

1 Introduction

Preliminary results of the investigation into the electromagnetic (EM) shielding properties of the Karoo soil are presented. The South African pathfinder to host the Square Kilometre Array (SKA) is known as MeerKAT and is to be located near Carnarvon in the Karoo (Northern Cape). The extremely sensitive radio receivers need to be situated in a radio quiet zone, and the levels of unwanted signal attenuation by burying cables and bunkers containing "noisy" electronic equipment are looked at. This research therefore investigates the use of the Karoo soil to further assist in the radio frequency interference (RFI) mitigation by considering its EM shielding properties. This is done by measuring the attenuation of induced signals on cables buried at various depths under ground. The complex permittivity of a soil sample is furthermore extracted in the high frequency (HF) laboratory of the University of Stellenbosch using methods described in the following sections.

2 Metrology

The measurement methods considered are based on the *Transmission/Reflection* (TR) and *Short-Circuit Line* (SCL) permittivity measurements discussed by *Baker-Jarvis* in [1]. In this work a procedure for obtaining complex permittivity from scattering equations, which is stable over the frequency spectrum, is presented. This procedure furthermore minimizes instability by setting the permeability to unity, and allows for measurements on samples of arbitrary length.

Considering the above mentioned methods, a dielectric sample is placed in a waveguide or coaxial line and the scattering parameters (S-parameters) are measured using a vector network analyser (VNA) or automatic network analyser (ANA). The scattering equations then relate measured S-parameters to the permittivity and permeability of the material. The TR procedure provides us with more data than in the SCL method as all four S-parameters are available. From [1] it is seen that the equations are generally over-determined and can be solved in various ways.

Work in this field was also done by Nicholson and Ross [2] and Weir [3] who introduced procedures for obtaining broadband measurements both in the time and frequency domain. The Nicholson-Ross-Weir (NRW) procedure combines the S-parameter equations in such a way that the system of equations can be decoupled. This procedure then yields an explicit equation for the permittivity and permeability as a function of the S-parameters. Although the compact form of these equations are elegant, it is not well behaved for low-loss materials at frequencies corresponding to multiples of half wavelength in the sample [1]. The *Baker-Jarvis* procedure discussed in [1] yields a procedure for obtaining complex permittivity from the scattering equations that are stable over the frequency spectrum by assuming the permeability at unity. This allows measurements to be taken over arbitrary sample lengths, and the procedure is used in this research for determining the complex permittivity of the Karoo soil.

2.1 Short-Circuit Line Method

The short-circuit line (SCL) method is a 1-port measurement using either a slotted line apparatus or a vector network analyser (VNA). The short circuit can either be fixed or movable, allowing for the dielectric sample to be in a strong electric or strong magnetic field region. Only the VNA technique is discussed in this report. Using a VNA, a sample is placed in either a coaxial line or waveguide where the reflection coefficient (S_{11}) is measured as show in figure 1.

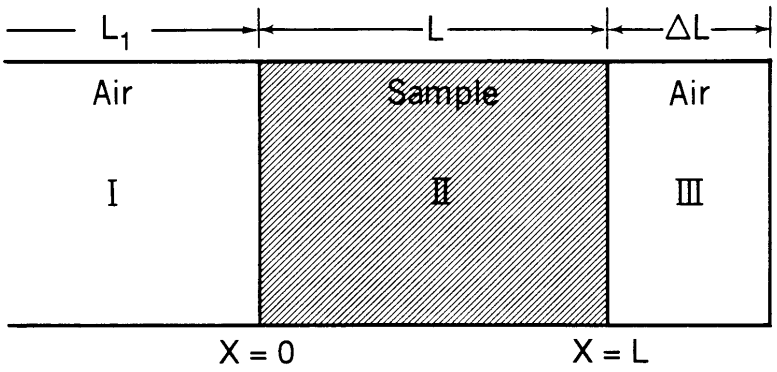

Figure 1: Transmission line with short-circuit termination [1]

The permittivity is determined using iterative procedures to solve an transcendental equation which involves the sample length, sample position and reflection coefficient [1].

2.1.1 Reflection Coefficient Method

As mentioned above, this method uses a VNA to measure the reflection coefficient (S_{11}) scattering parameter. Consider the sample in a transmission line with three regions (I, II and III) as in figure 1. The electric fields, when only assuming the dominant mode, can be given by

$$E_I = \exp(-\gamma_0 x) + C_1 \exp(\gamma_0 x) \tag{1}$$

$$E_{II} = C_2 \exp(-\gamma x) + C_3 \exp(\gamma x) \tag{2}$$

$$E_{III} = C_4 \exp(-\gamma_0 (x - L)) + C_5 \exp(\gamma_0 (x - L)) \tag{3}$$

where γ and γ_0 are the propagation constants in the material and in a vacuum respectively given by

$$\gamma = j\sqrt{\frac{\omega^2 \mu_R^* \epsilon_R^*}{c_{vac}^2} - \left(\frac{2\pi}{\lambda_c}\right)^2} \tag{4}$$

$$\gamma_0 = j\sqrt{\left(\frac{\omega}{c_{lab}}\right)^2 - \left(\frac{2\pi}{\lambda_c}\right)^2} \tag{5}$$

and ϵ and μ are the permittivity and permeability given by

$$\epsilon = [\epsilon'_R - j\epsilon''_R]\,\epsilon_0 = \epsilon^*_R\epsilon_0 \tag{6}$$

$$\mu = [\mu'_R - j\mu''_R]\,\mu_0 = \mu^*_R\mu_0 \tag{7}$$

In the above equations $j = \sqrt{-1}$, c_{vac} and c_{lab} are the speed of light in a vacuum and the laboratory, ω is the angular velocity, λ_c is the cutoff wavelength, ϵ_0 and μ_0 are the permittivity and permeability of vacuum, ϵ^*_R and μ^*_R are the complex permittivity and permeability of the material relative to a vacuum.

Transverse electromagnetic fields with no radial dependence are assumed in equations 1 to 3. The coefficients are determined by imposing the following boundary conditions at the interfaces (x=0 and x=L):

- Tangential component of *electric field* is continuous at sample interface
- Tangential component of *magnetic field* is continuous at sample interface
- The *electric field* is null at the short-circuit

The equations for the coefficients are obtained by imposing the boundary conditions and are given in [1] as follows:

$$1 + C_1 = C_2 + C_3 \tag{8}$$

$$C_2\exp(-\gamma L) + C_3\exp(\gamma L) = C_4 + C_5 \tag{9}$$

$$\frac{\gamma_0\mu}{\gamma\mu_0}\,[C_1 - 1] = C_3 - C_2 \tag{10}$$

$$\frac{\gamma\mu_0}{\gamma_0\mu}\,[C_2\exp(-\gamma L) - C_3\exp(\gamma L)] = C_4 - C_5 \tag{11}$$

$$C_5 = -\delta C_4 \tag{12}$$

where

$$\delta = \exp(-2\gamma_0\Delta L) \tag{13}$$

and ΔL is the distance from the sample to the short-circuit. Equations 8 to 12 then lead to the following system of equations:

$$C_1 - C_2 - C_3 = -1 \tag{14}$$

$$\eta C_2 + \frac{C_3}{\eta} + (\delta - 1)\,C_4 = 0 \tag{15}$$

$$C_1 + \beta C_2 - \beta C_3 = 1 \tag{16}$$

$$\beta\eta C_2 - \frac{\beta}{\eta}C_3 - C_4\,(1 + \delta) = 0 \tag{17}$$

where

$$\beta = \frac{\gamma\mu_0}{\mu_0\gamma} \tag{18}$$

$$\eta = \exp(-\gamma L) \tag{19}$$

It is noted in [1] that $1/\beta$ is an effective impedance and that the matrix form of these equations is presented by:

$$\begin{pmatrix} 1 & -1 & -1 & 0 \\ 0 & \eta & \frac{1}{\eta} & \delta - 1 \\ 1 & \beta & -\beta & 0 \\ 0 & \beta\eta & -\frac{\beta}{\eta} & -(1+\delta) \end{pmatrix} \begin{pmatrix} C_1 \\ C_2 \\ C_3 \\ C_4 \end{pmatrix} = \begin{pmatrix} -1 \\ 0 \\ 1 \\ 0 \end{pmatrix} \tag{20}$$

The solution of equations 14 to 17 yields the following equation for the permittivity in terms of the reflection coefficient, $\rho = S_{11} = C_1$, with the sample located a distance ΔL from the short circuit:

$$S_{11} = \rho = \frac{-2\beta\delta + \left[(\delta+1) + (\delta-1)\beta^2\right]\tanh\gamma L}{2\beta + \left[(\delta+1) + (\delta-1)\beta^2\right]\tanh\gamma L} \tag{21}$$

2.2 Transmission/Reflection Method

The transmission/reflection (TR) measurement consists of a dielectric sample subjected to an incident electromagnetic field when placed in a coaxial line or waveguide as shown in figure 2. This is typically transverse electromagnetic (TEM) and transverse electric (TE_{10}) modes for the coaxial line and waveguide respectively. The scattering equations are found by analysis of the electric field at the sample interfaces. Assuming electric fields E_I, E_{II} and E_{III}, with a time dependence of $\exp(j\omega t)$ in the regions I, II and III, the spatial distribution of the electric field for an incident normalised to 1 is given by:

$$E_I = \exp(-\gamma_0 x) + C_1\exp(\gamma_0 x) \tag{22}$$

$$E_{II} = C_2\exp(-\gamma x) + C_3\exp(\gamma x) \tag{23}$$

$$E_{III} = C_4\exp(-\gamma_0 x) \tag{24}$$

where γ and γ_0 is the propagation constants in the material and in a vacuum respectively given by

$$\gamma = j\sqrt{\frac{\omega^2\mu_R^*\epsilon_R^*}{c^2} - \left(\frac{2\pi}{\lambda_c}\right)^2} \tag{25}$$

$$\gamma_0 = j\sqrt{\left(\frac{\omega}{c}\right)^2 - \left(\frac{2\pi}{\lambda_c}\right)^2} \tag{26}$$

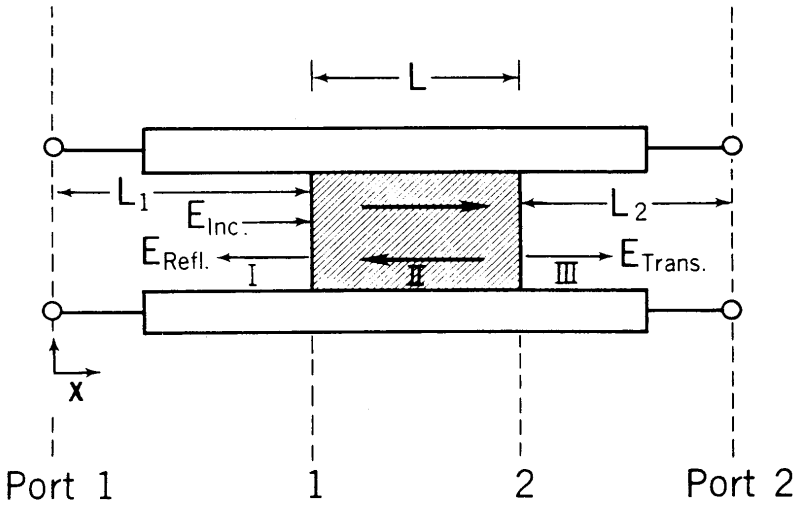

Figure 2: The transmission/reflection method with a dielectric sample in a transmission line with incident and reflected electric field distribution regions I, II and III [1]

and ϵ and μ are the permittivity and permeability given by

$$\epsilon = [\epsilon'_R - j\epsilon''_R]\,\epsilon_0 = \epsilon^*_R \epsilon_0 \tag{27}$$

$$\mu = [\mu'_R - j\mu''_R]\,\mu_0 = \mu^*_R \mu_0 \tag{28}$$

The coefficients C_i are again determined by applying the boundary conditions that the tangential component of the electric field is continuous across the interfaces. From [1] it is seen that the tangential component can be calculated from Maxwell's equations given an electric field with only a radial component.

$$E_I(x = L_1) = E_{II}(x = L_1) \tag{29}$$

$$E_{II}(x = L_1 + L) = E_{III}(x = L_1 + L) \tag{30}$$

If no surface currents are generated, the boundary condition that the tangential component of the magnetic field is continuous across the interfaces holds. From [1] it is seen that the tangential component can be calculated from Maxwell's equations given an electric field with only a radial component, such that:

$$\frac{1}{\mu_0}\frac{\partial E_I}{\partial x}(x = L_1) = \frac{1}{\mu_0}\frac{\partial E_{II}}{\partial x}(x = L_1) \tag{31}$$

$$\frac{1}{\mu_0}\frac{\partial E_{II}}{\partial x}(x = L_1 + L) = \frac{1}{\mu_0}\frac{\partial E_{III}}{\partial x}(x = L_1 + L) \tag{32}$$

Solving equations 22 to 24 subject to the boundary conditions, the expressions for the measured S-parameters of a two-port device is given by:

$$S_{11} = R_1^2 \left[\frac{\Gamma(1-z^2)}{1-\Gamma^2 z^2} \right] \tag{33}$$

$$S_{22} = R_2^2 \left[\frac{\Gamma(1-z^2)}{1-\Gamma^2 z^2} \right] \tag{34}$$

$$S_{21} = R_1 R_2 \left[\frac{z(1-\Gamma^2)}{1-\Gamma^2 z^2} \right] \tag{35}$$

where

$$R_1 = \exp(-\gamma_0 L_1) \tag{36}$$

$$R_2 = \exp(-\gamma_0 L_2) \tag{37}$$

R_1 and R_2 are the respective reference plane transformation expressions, while L_1 and L_2 are the distances from the calibration reference planes to the sample ends [1]. The reflection coefficient, Γ, is given by equation 38.

$$\Gamma = \frac{\frac{\gamma_0}{\mu_0} - \frac{\gamma}{\mu}}{\frac{\gamma_0}{\mu_0} + \frac{\gamma}{\mu}} \tag{38}$$

S_{21} for an empty sample holder is given in [1] as

$$S_{21}^o = R_1 R_2 \exp(-\gamma_0 L) \tag{39}$$

For non-magnetic materials equations 33, 34 and 35 have ϵ_R', ϵ_R'', L, R_1 and R_2 as unkown quantities. Seeing that S_{21} and S_{12} are equivalent for isotropic materials, there are four complex equations 33, 34, 35 and 39 as well as the equations for length of the air line. It is shown in [1] that the system of equations are overdetermined and that it is possible to solve these equations in various combinations.

2.2.1 Nicholson-Ross-Weir

Nicholson-Ross-Weir (NRW) combined the S_{11} and S_{21} measurements and discovered a formula for the permittivity and permeability. It is shown in [1] that this procedure works well at frequencies that are now a multiple of a half wavelength in the material. At these latter frequencies, the procedure completely breaks down. In the NRW method the reflection coefficient, Γ_1, is given explicitly in terms of the scattering parameters such that

$$\Gamma_1 = X \pm \sqrt{X^2 - 1} \tag{40}$$

where

$$X = \frac{1 - V_1 V_2}{V_1 - V_2} \tag{41}$$

and

$$V_1 = S_{21} + S_{11} \tag{42}$$

$$V_2 = S_{21} - S_{11} \tag{43}$$

The correct root is chosen in equation 40 by requiring that $|\Gamma_1| \leq 1$. The NRW method then yields the following transmission coefficient:

$$z_1 = \frac{S_{11} + S_{21} - \Gamma_1}{1 - (S_{11} + S_{21})\,\Gamma_1} \tag{44}$$

with

$$\frac{1}{\Lambda^2} = -\left[\frac{1}{2\pi L}\ln(\frac{1}{z_1})\right]^2 \tag{45}$$

The permeability is then given by equation 46, while the permittivity is given by equation 47.

$$\mu_R^* = \frac{1 + \Gamma_1}{(1 - \Gamma_1)\,\Lambda\sqrt{\frac{1}{\lambda_0^2} - \frac{1}{\lambda_c^2}}} \tag{46}$$

$$\epsilon_R^* = \frac{\lambda_0^2}{\mu_R^*}\left[\frac{1}{\lambda_c^2} - [\frac{1}{2\pi L}\ln(\frac{1}{z_1})]^2\right] \tag{47}$$

In equations 46 and 47 λ_0 and λ_c is the free space wavelength and cutoff wavelength respectively. In the work in [1] it is assumed that $\mu_R^* = 1$ to remove the ambiguity in the logarithm branch. In order to choose the correct root in equation 45 it is necessary to compare the measured group delay to the calculated group delay. In [1] it is seen that the calculated group delay is related to the change in wavenumber, k, with respect to angular frequency

$$\tau_{group,calc} = L\frac{d}{df}\sqrt{\frac{\epsilon_R^*\mu_R^*}{\lambda_0^2} - \frac{1}{\lambda_c^2}} \tag{48}$$

The measured group delay is given by

$$\tau_{group,measured} = -\frac{1}{2\pi}\frac{d\phi}{df} \tag{49}$$

where ϕ is the measured phase. To determine the correct root, the calculated group delays are found from equation 49 for various values of n in the logarithm

term in equation 45, using $\ln z = \ln|z| + j\,(\theta + 2\pi n)$ where $n = 0, \pm 1, \pm 2, \ldots$, and compared to the measured value in equation 49. The comparison yields the correct value for n.

2.2.2 Baker-Jarvis

From [1] it is seen that for cases where the sample length and reference plane positions are known to a high accuracy, taking various linear combinations of the scattering equations and solving these equations in an *iterative* manner yields a stable solution for samples of an arbitrary length. This is unlike the NWR method where, at points corresponding to half wavelength, the S-parameter $|S_{11}|$ gets very small. For a small S_{11} the uncertainty in the measurement of the phase of S_{11} on a VNA is large. The uncertainties dominate the solution at these frequencies, and the NWR solutions is divergent at integral multiples of a half wavelength. Using the *Baker-Jarvis* method in [1], this singularity behaviour can be minimized in cases where the permeability is known *a priori*.

A useful combination of the S-parameters is given in [1] as:

$$\frac{1}{2}\left([S_{12} + S_{21}] + \beta[S_{11} + S_{22}]\right) = \frac{z(1-\Gamma^2) + \beta\Gamma(1-z^2)}{1 - z^2\Gamma^2} \tag{50}$$

The S-parameters to be used in equation 50 need to be transformed from the calibration plane to the sample face using equations 36 and 37. In equation 50, β is a weighting function for the S-parameters. It is a constant which varies as a function of sample length, uncertainty of S-parameters and loss characteristics of the material. For low-loss materials the S_{21} signal is strong, so we can set $\beta = 0$. For materials with high loss, S_{11} dominates and large values of β can be set. A general relation for β is given by the ratio of the uncertainty in S_{21} divided by the uncertainty in S_{11}.

3 Calibration

A measurement calibration is defined in [4] as a process that mathematically derives the error model for the network analyser. This error model is an array of vector coefficients used to establish a fixed reference plane of zero phase shift, zero magnitude and known impedance. The calibration is achieved using a *calibration kit* that is a set of physical devices called standards. Each standard has a known magnitude and phase response as a function of frequency.

A problem with making network measurements is the need to separate the effects of the transmission medium from the device characteristics. In most microwave measurements, systematic errors are the most significant source of measurement uncertainty. These errors are often caused by imperfections in the test equipment and setup. If these errors do no vary with time, they can be characterised and mathematically removed during the measurement process [4].

3.1 Two-Port Calibration

A full 2-port calibration includes both *forward* and *reverse* error terms, and the calibration standards will be applied to both ports of the VNA during the calibration procedure. In conventional 2-port calibrations, three known impedance standards and a single transmission standard are required. For a coaxial system this typically includes a zero-electrical-length *short*, a shielded *open* and matched *load* terminations.

3.2 TRL Calibration

The Thru-Reflect-Line (TRL) calibration relies on the characteristic impedance of a short transmission line, rather than a set of discrete impedance standards. From two sets of two-port measurements that differ by this short length transmission line and two reflection measurements, the full 12-term error model can be determined [4]. The TRL calibration refers to three basic steps in the calibration process:

1. THRU
   A connection between port 1 and port 2 either directly, or with a short piece of transmission line
2. REFLECT
   Connection of an identical high reflection coefficient device to each port
3. LINE
   Insertion of a short length of transmission line between port 1 and port 2. A different line length is required for the THRU and LINE calibration process.

The upper and lower cut-off frequencies of the waveguide is given in [4] by equations 51 and 52 respectively. This is calculated for a WR-90 waveguide with inside width dimension $a = 2.286$ cm.

$$f_{cut-off(lower)} = \frac{c}{2a} = \frac{2.997 \times 10^8 \text{ m/s}}{2 \times 2.286 \times 10^{-2} \text{ m}} = 6.55 \text{ GHz} \tag{51}$$

$$f_{cut-off(upper)} = 2 \times f_{cut-off(lower)} = 13.11 \text{ GHz} \tag{52}$$

The linear delay due to the lenght of the LINE section is given by equation 53, and calculated for an offset length of $l = 1$ cm.

$$\text{Linear Delay} = \frac{l\sqrt{\epsilon_r}}{c} = \frac{1 \times 10^{-2} \text{ m}\sqrt{1.00065}}{2.997 \times 10^8 \text{ m/s}} = 33.38 \text{ ps} \tag{53}$$

In a waveguide the group velocity varies with frequency due to dispersion as a function of the cut-off frequency. The actual delay is given by equation 54 and is calculated for a measurement frequency of $f = 10$ GHz where f_{co} is the lower

cut-off frequency.

$$\text{Actual Delay} = \frac{\text{Linear Delay}}{\sqrt{1-(f_{co}/f)^2}} \tag{54}$$

$$= \frac{33.38 \text{ ps}}{\sqrt{1-(6.55 \text{ GHz}/10 \text{ GHz})^2}} = 44.17 \text{ ps}$$

From [4] it is seen that the TRL LINE insertion phase requirement for a good calibration should be between 20^o and 120^o. This is calculated for the 1cm LINE for a measurement frequency of $f = 10$ GHz using:

$$\text{Degrees} = \frac{360^o \times f}{c}\left(\sqrt{1-(f_{co}/f)^2}\right) l \tag{55}$$

$$\text{Degrees} = \frac{360^o \times 10 \times 10^9 \text{ Hz}}{2.997 \times 10^8 \text{ m/s}}\left(\sqrt{1-(6.55/10)^2}\right)\left(1 \times 10^{-2} \text{ m}\right) = 90.77^o$$

.

4 Waveguide Measurements

Work on microwave material characterisation has been a well published topic in the past few decades. The primary objective is to determine the real and imaginary parts of the relative complex permittivity of a dielectric given by equation 56.

$$\epsilon_r = \epsilon_r' - j\epsilon_r'' \tag{56}$$

The real part of the of the relative permittivity is known as the dielectric constant, while the imaginary part is known as the loss factor [5]. The ratio between the loss factor and dielectric constant is called the loss tangent, and for dielectric materials with $\epsilon_r'' \geq 0$ and ϵ_r" $\gg \epsilon_r''$ is give by

$$\tan\delta = \frac{\epsilon_r''}{\epsilon_r'} \tag{57}$$

The measurement setup diagram is similar to that in [6] and is shown in figure 3. Measurements were made in the *S-band* and *X-band* frequency ranges using the *WR284* and *WR90* waveguides as discussed in the following section.

4.1 WR284 & W90 Standards

Both the *WR284* and *WR90* waveguide standards were used for S-parameter measurements to perform complex permittivity extraction on various dielectric samples using the transmission/reflection (TR) procedure. The dimensions of the S-band and X-band waveguides are given in table 1, while the extraction procedure and mathematics were explained in some detail in section 2. The experimental arrangement using the HP8510 VNA and WR90 X-band waveguide and sample holder is

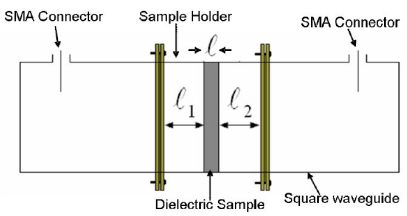

Figure 3: Waveguide with dielectric sample of thickness l placed at the centre of sample holder [6]

shown in figure 4. The verification procedure for the TR method consists of measuring the permittivity of air in the empty sample holder before each measurement of the dielectric sample, and comparing those results to a reference set. The magnitude of the measured S-band S-parameters of the air sample is shown in figure 5 where it is also compared to values computed using a commercial computational electromagnetic (CEM) software package called CST. The computation is discussed in greater detail in section 5. The corresponding phase plots of the S-parameters is shown in Appendix A.

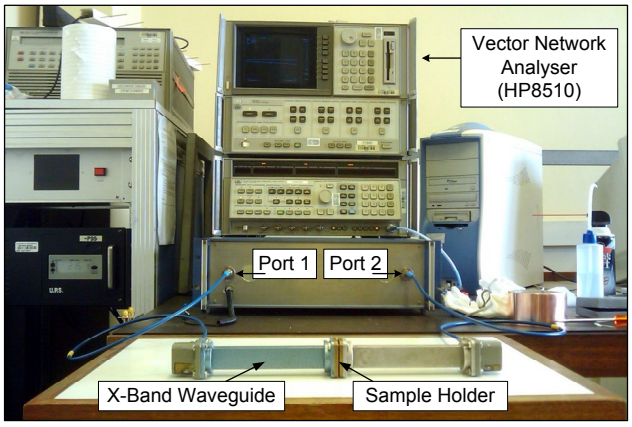

Figure 4: S-parameter measurements using an HP8510 Vector Network Analyser with WR90 X-band waveguides and soil sample holder

The S-parameters measured in the S and X-bands are then used in the iterative Baker-Jarvis (BJ) extraction method, discussed in section 2.2.2, to calculate the real and imaginary values of the complex permittivity of the air sample. The results are shown in figure 6 and 7 for the real and imaginary values respectively. This was done for an initial value of $\beta = 1$. For additional confirmation of the metrological techniques, similar measurements in the S-band were made with a dielectric sample of teflon which has well published data. The results of the complex permittivity extraction is shown in figures 26 and 27 in Appendix B. The data extraction for teflon yielded $\epsilon_r' \approx 2.2$ and $\tan\delta \approx 0.009$ which agrees well with published data.

WR Size	Freq. Band	Start Freq. [GHz]	Stop Freq. [GHz]	TE10 Cutoff [GHz]	Inside Dim. "a" [cm]	Inside Dim. "b" [cm]	Wall Thick. [cm]
284	S	2.60	3.95	2.078	7.710	3.403	0.200
90	X	8.20	12.4	6.557	2.286	1.016	0.125

Table 1: Dimensions of the *S-band* and *X-band* waveguide standards

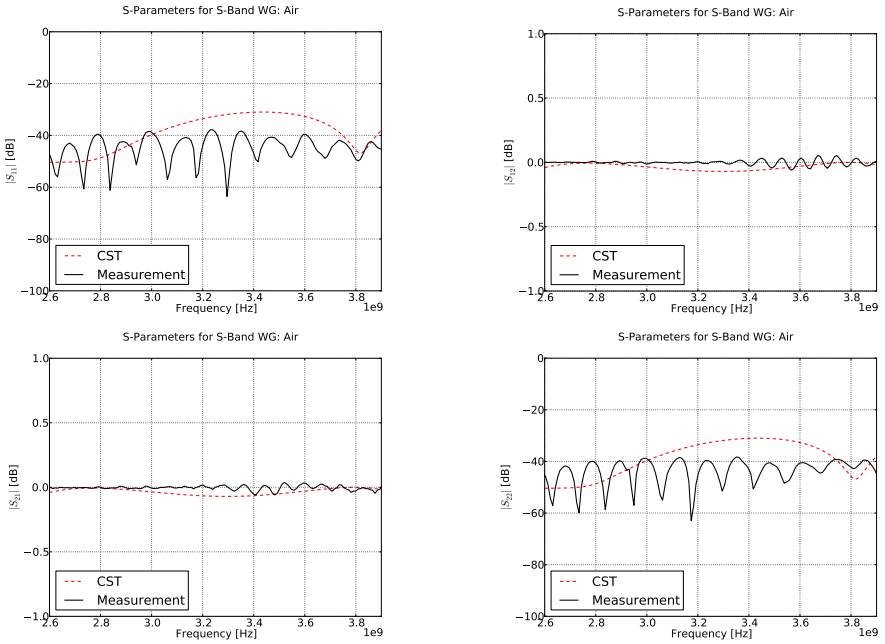

Figure 5: S-Parameters of air sample measured with S-band waveguide (Magnitude)

Next, S-parameters of various soil samples from the Karoo site for the KAT-7 and MeerKAT were measured. This was done for the S-band and X-band, and the real and imaginary results for the extracted complex permittivity of the Karoo soil sample is shown in figures 8 and 9 respectively. The data extraction for Karoo soil yielded $\epsilon_r' \approx 3.8$, $\epsilon_r'' \approx 0.29$ and $\tan\delta \approx 0.076$. The extracted complex permittivity results were confirmed by placing it in a numerical model and comparing the computed and measured S-parameters. The computed S-parameters were then used in the Baker-Jarvis extraction method where good agreement was found between the computed and measured complex permittivity values. This is discussed in detail in section 5.

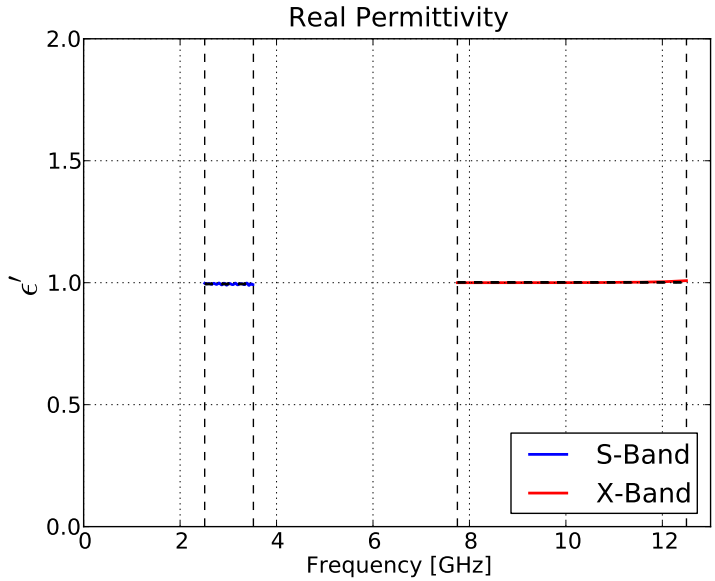

Figure 6: Extracted real value of the complex permittivity of air using the BJ method in S-band and X-band

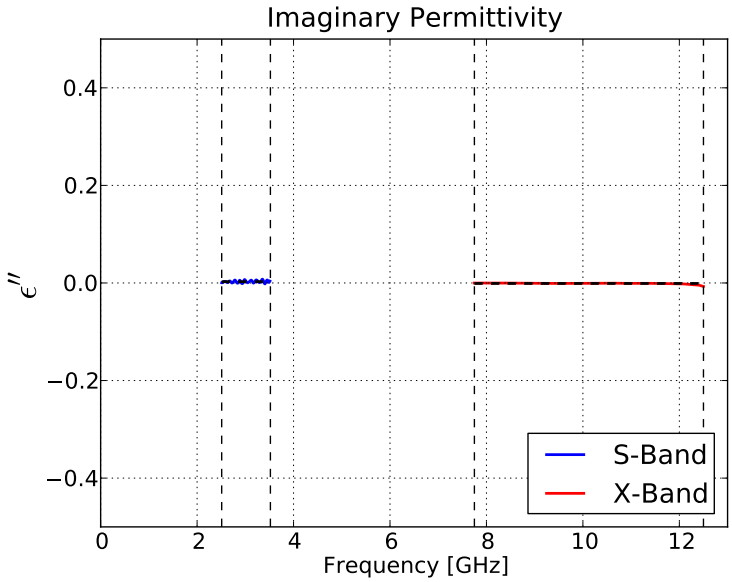

Figure 7: Extracted imaginary value of the complex permittivity of air using the BJ method in S-band and X-band

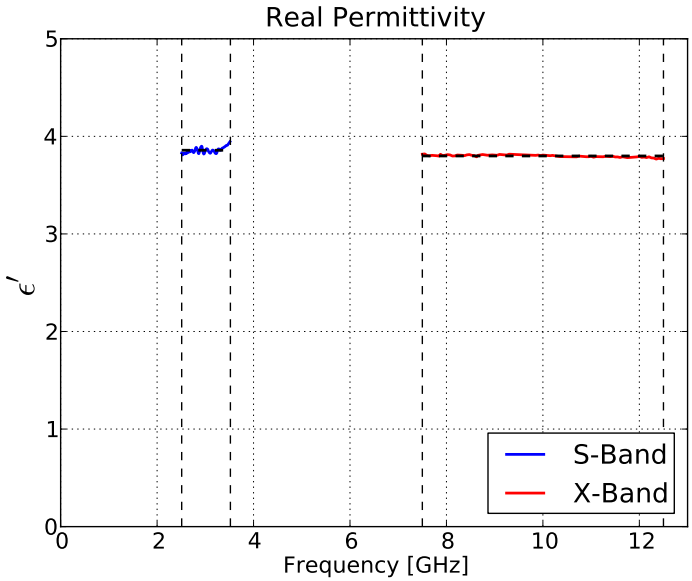

Figure 8: Real value of derived S-band and X-band complex permittivity of Karoo soil

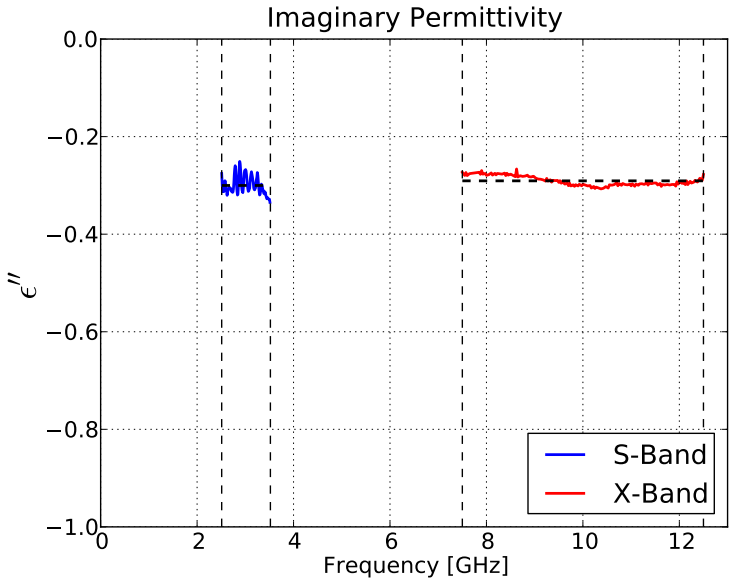

Figure 9: Imaginary value of derived S-band and X-band complex permittivity of Karoo soil

5 Computation

A commercial 3D electromagnetic (EM) field solver called *Computer Simulation Technology* (CST) [7], which is based on the *finite difference time domain* (FDTD) numerical method, was used in this study to confirm the S-parameters measured for a dielectic sample with a certain complex permittivity. Waveguide measurements and computation were used to extract the complex permittivity values, which in turn were used in an experiment and numerical model using X-band horn antennas to compute the relative attenuation of the dielectric sample. This is discussed in detail in sections 5.1 and 5.2 respectively.

5.1 X-Band Waveguide

The CST computational model of the X-band WR-90 waveguide and dielectric sample holder is shown in figure 10.

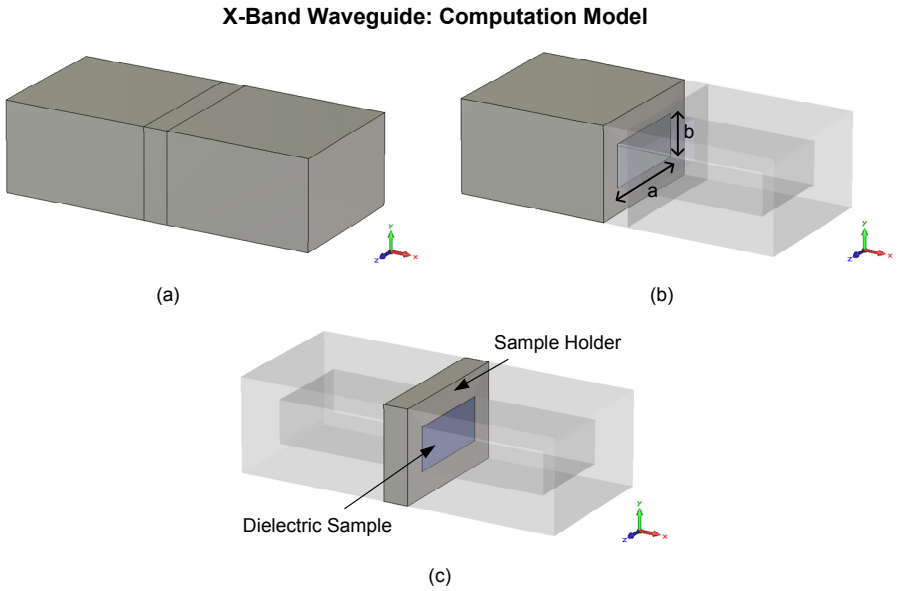

Figure 10: CST computational model of X-band waveguide

Two waveguide ports were defined in CST with only a TE_{10} excitation mode present. The waveguide port definitions and transverse electric wave mode (TE_{10}) is shown in figure 11.The complex permittivity values and loss tangent extracted from the measurements discussed in section 4.1 were insterted into the CST dielectric material editor. The S-parameters of the waveguide computational model in figure 10 were then compared to the measured S-parameters. This was done not only done for the Karoo soil sample, but also to confirm the computational models for air and teflon which has well published complex permittivity data. The

magnitude of the computed and measured S-parameters in the S-band frequency range for a value of $\epsilon_r' = 3.8$ is shown in figure 12, while the phase plots are shown in Appendix A figure 24.

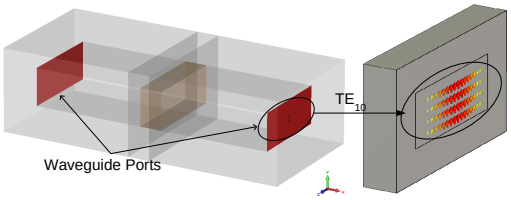

Figure 11: Waveguide port definitions and TE_{10} mode

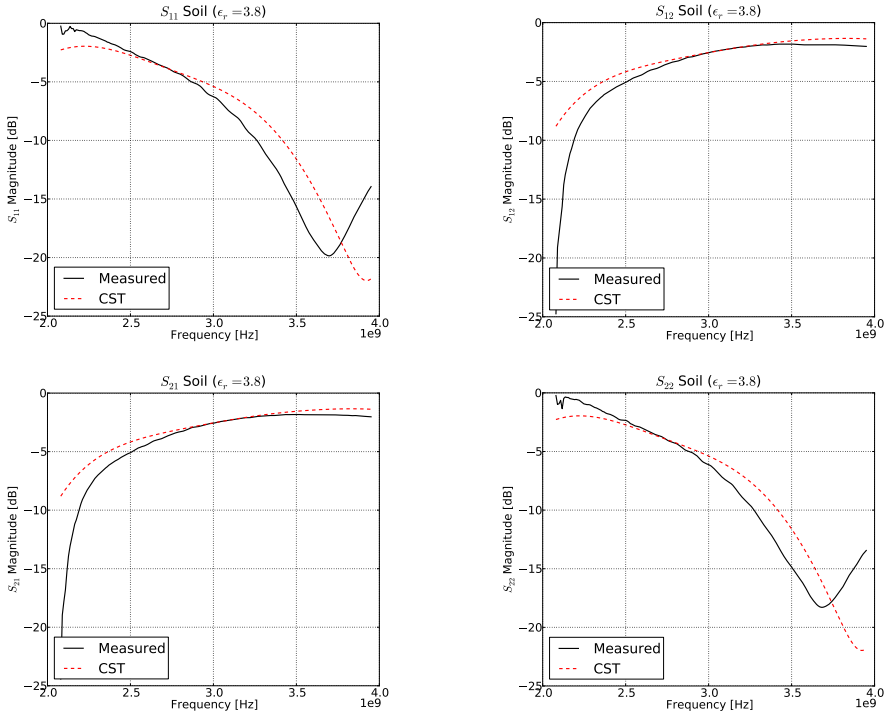

Figure 12: S-Parameters of Karoo soil sample measured with S-band waveguide (Magnitude)

5.2 X-Band Horn Antenna

The CST computational model of a X-band horn antenna with it's radiation pattern and half power beam width (HPBW) calculation is shown in figure 13. The antenna is modelled to confirm the results of the experimental arrangement to measure the

relative attenuation of dielectric samples.

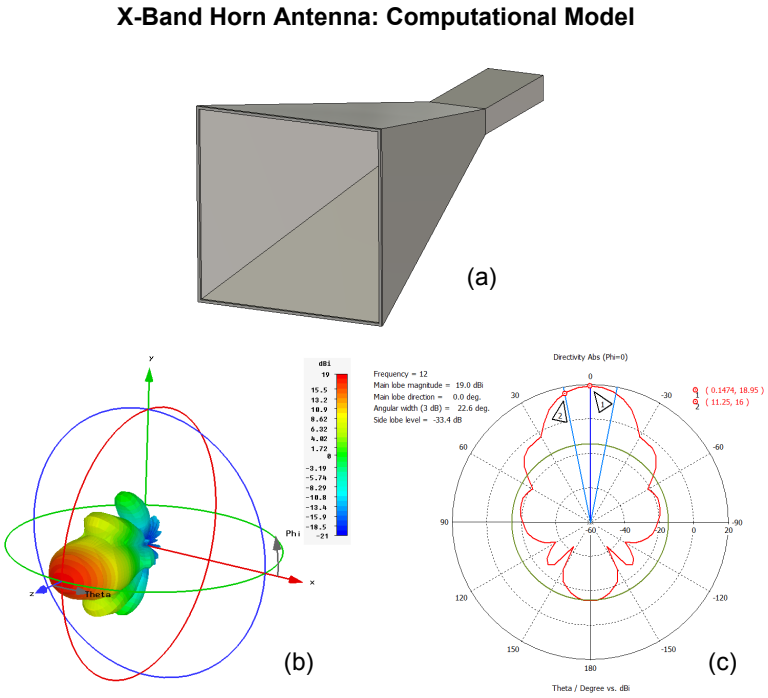

Figure 13: CST computational model of (a) the X-band horn antenna with its (b) radiation pattern and (c) directivity and HPBW

Two horn antennas facing each other are placed an equal distance from a dielectric sample (in this case Karoo soil) as shown in figure 14. One antenna (port 1) transmits a signal in the frequency range between 8 GHz and 12 GHz, while the other antenna (port 2) receives the transmitted signal. Dielectric samples of various thicknesses are placed between the antennas and the relative attenuation of the signal due to the sample is measured as a S_{21} S-parameter. The antennas are placed a distance greater than R away from the sample such that it is in the far field region given by:

$$R \approx \frac{2D^2}{\lambda} \tag{58}$$

The sample dimensions were chosen to ensure that the half power beam width (HPBW) of the transmitting antenna illuminated the sample area. The attenuated electromagnetic (EM) signal is visualised using the CST Microwave Studio EM solver as seen in figure 15. The measurements were made in the anechoic chamber at the University of Stellenbosch, with the measured and computed results shown in figure 16. These results agree well with the predicted attenuation values (given the

extracted complex permittivity values) discussed in section 7. The computational model confirmed the X-band measurements and was furthermore used to investigate the lower frequency components. This was done seeing that the physical sample size to accomodate the HPBW of lower range antennas would be impracticle. The measured, computed and predicted attenuation values [dB/m] is shown in figure 22.

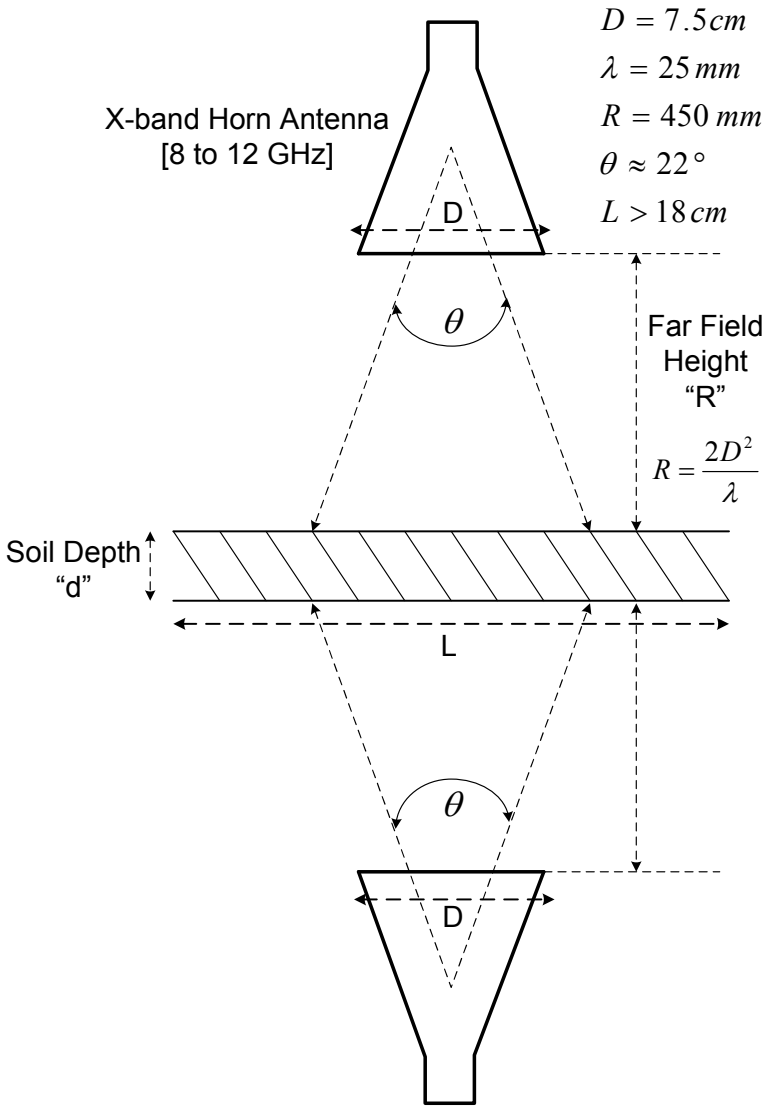

Figure 14: Experimental setup with X-band horn antennas and Karoo soil sample

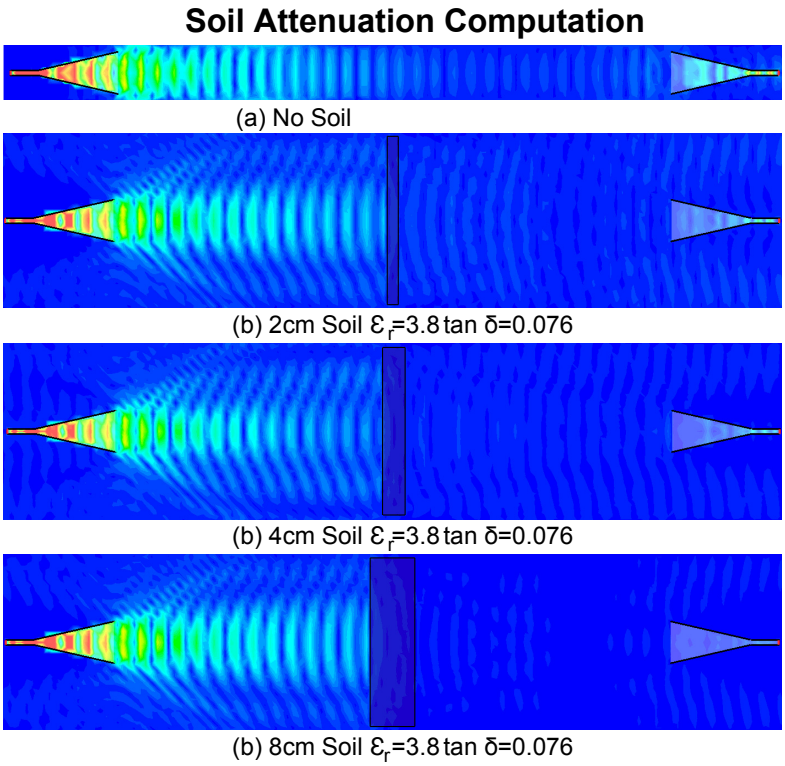

Figure 15: CST computational model of two X-band horn antennas with various soil samples

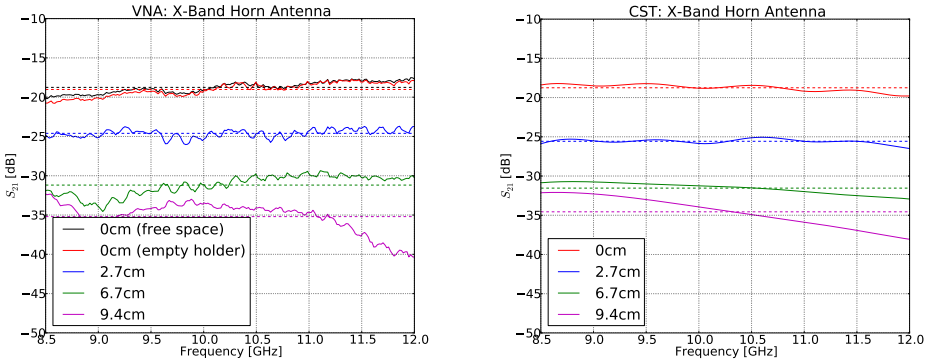

Figure 16: (a) VNA Measured S-Parameters (b) CST Computed S-Parameters

6 Karoo Measurements

6.1 Experimental Setup

Measurements using a signal generator, log periodic dipole antenna (LPDA), spectrum analyzer and an exposed coaxial RG58/U cable (of which the outer shielded braid was removed) were all used for the measurements of the signal attenuation due to the Karoo soil. The signal generator was set to a level of 10dBm over the frequency range between 300 MHz and 3 GHz. The LDPA has a gain of roughly 6dB over this frequency range. The exposed coaxial cable connected to the spectrum analyzer was then burried at various depths below the Karoo soil while being illuminated by the signal generator and LPDA from above ground. The signal radiated from the antenna induces a current on the exposed centre conductor of the coaxial cable, which is then measured with the spectrum analyzer at various depth below ground. The schematic of the experimental arrangement is shown in figure 17, with photos of the actual measurement in figure 18.

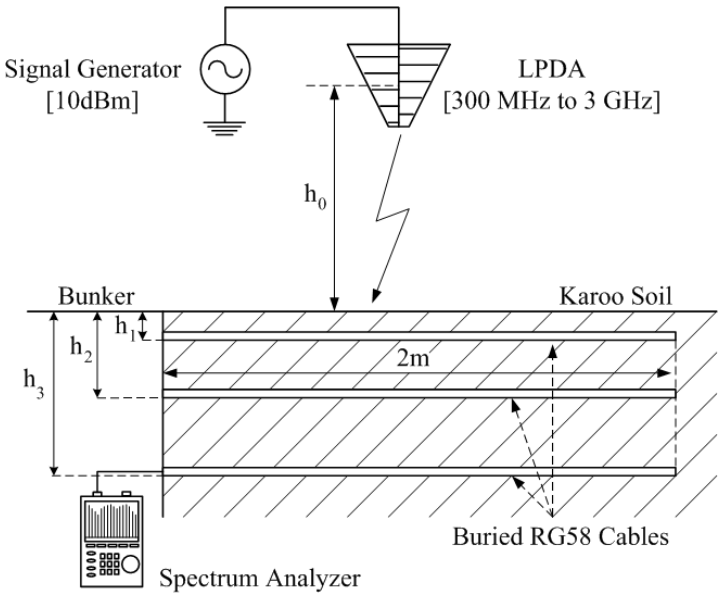

Figure 17: Setup diagram of Karoo measurements of exposed cable buried at various depths below ground level [8]

The location for the experiment was chosen at the Losberg site base complex to measure the shielding properties of typical soil that will be used at the KAT-7 and MeerKAT sites. The site was furthermore chosen for convenience as a brick bunker is located at this site where all the fibre optic ducts used for data transfer from the KAT-7 site comes together. The bunker with manhole covering as well as the LPDA mounted on a tripod is shown in figure 17. Three extra fibre optic ducts with a length of 1 m were buried directly above each other at depths of 20, 50

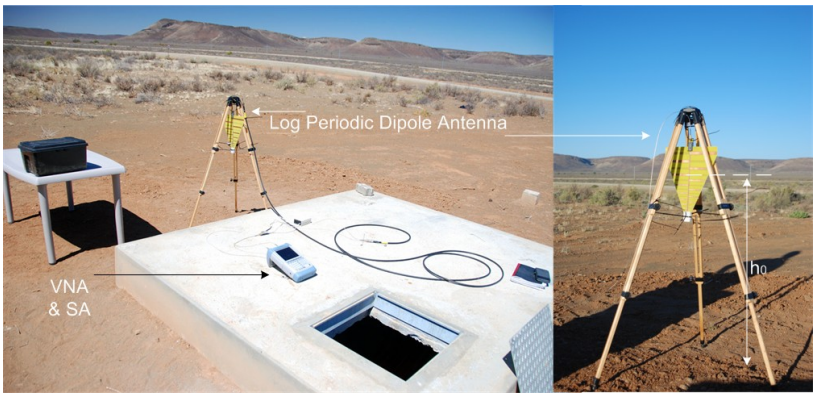

Figure 18: Measurement setup in Karoo consisting of LPDA above ground and exposed conductor at various depths below ground

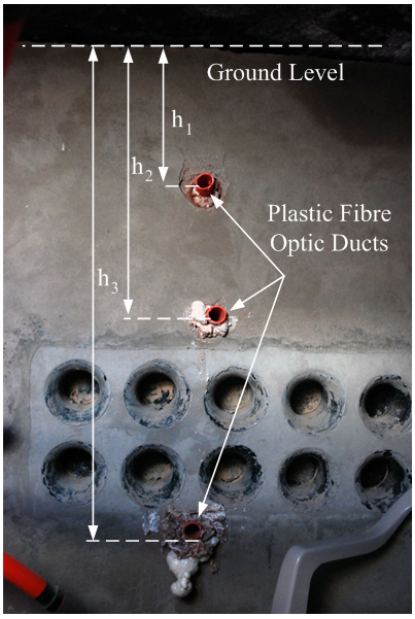

Figure 19: (a) Fibre optic ducts at depths of 20cm, 50cm and 100cm under ground (b) Measurements with R&S FSH8 spectrum analyzer

and 100 cm with the openings accessible from inside the bunker as shown in figure 19(a). The exposed RG58 coaxial cable and spectrum analyzer were then inserted at these various depths underground as shown in figure 19(b). Two measurement sets were completed. During the first, the height of the LPDA above ground was kept constant. This meant that only the depth of the cable and the distance to the LPDA was varied. This implies a constant air attenuation loss for all three depth measurements with the LPDA in the far field region. The second measurement was done by keeping the distance between the LPDA and device under test (DUT)/cable constant by varying the height of the antenna above ground. This implies a varying air and soil attenuation factor. Both of these results are shown and discussed in the following section.

6.2 Measurement Results

The measured results for the antenna at a constant height above the ground, while the depth of the exposed coaxial cable varies, are shown in figure 20 for a zoomed in frequency range of 500 MHz to 1 GHz. The measured results for the antenna a constant distance from the exposed coaxial cable (DUT) are shown in figure 21.

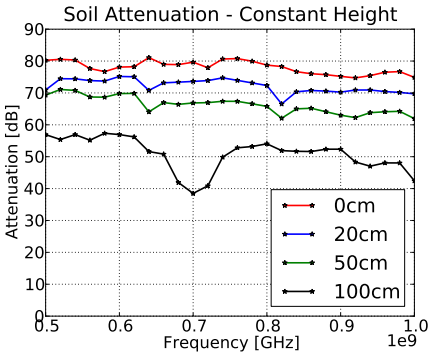

Figure 20: Measured results with LPDA at constant height above ground

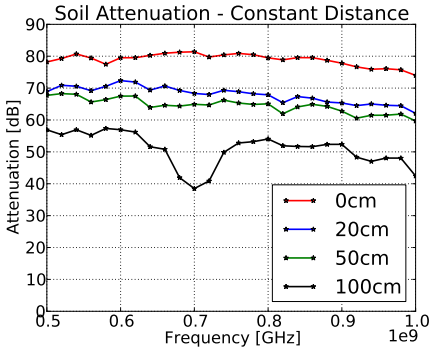

Figure 21: Measured results with LPDA at constant distance from DUT

On average a signal attenuation between 20 dB and 30 dB is seen for frequencies between 500 MHz and 1 GHz. These results agree well with the predicted values discussed in section 7. The higher frequency results using the R&S FSH4 as a vector network analyzer (VNA) to measure the S_{21} scattering parameter is shown in Appendix A figure 25. It is seen that for measurements above 1.5 GHz the 50 cm and 100 cm depth results are in the noise floor of the instrument. This gives an indication of the minimum attenuation level at that depth and frequency.

The results of the Karoo measurements in the frequency range between 500 MHz and 2 GHz (with a data curve fit), the laboratory results and curve fit between 8 GHz and 12 GHz, the computed values between 3.5 GHz and 12 GHz as well as the analytically predicted values over the whole range is shown in figure 22. The results are discussed in section 7.

7 Results and Discussion

The iterative complex permittivity extraction methods were discussed in detail in section 2, while the calibration procedures to accurately measure the waveguide and sample holder scattering parameters were investigated in section 3. The complex permittivity values of a dielectric sample were extracted using the waveguide measured S-parameters discussed in section 4, and then used in both computational models and experimental arrangements to derive the attenuation level [dB/m] of the Karoo soil sample as a function of frequency. The extracted complex permittivity values were also used in the analytical expression to predict the attenuation level over a frequency range. The attenuation in $[dB/m]$ is given in [9] and [10] equation 59.

$$\alpha = 8.686 \times \frac{2\pi f}{c} \sqrt{\frac{\epsilon'_S}{2}\left(\sqrt{1+\left(\frac{\epsilon''_S}{\epsilon'_S}\right)^2}-1\right)} \tag{59}$$

The predicted attenuation for the Karoo soil, with extracted values of $\epsilon'_r \approx 3.8$ and $\epsilon''_r \approx 0.29$ ($\tan\delta \approx 0.076$), is compared to measured and computed attenuation levels in figure 22.

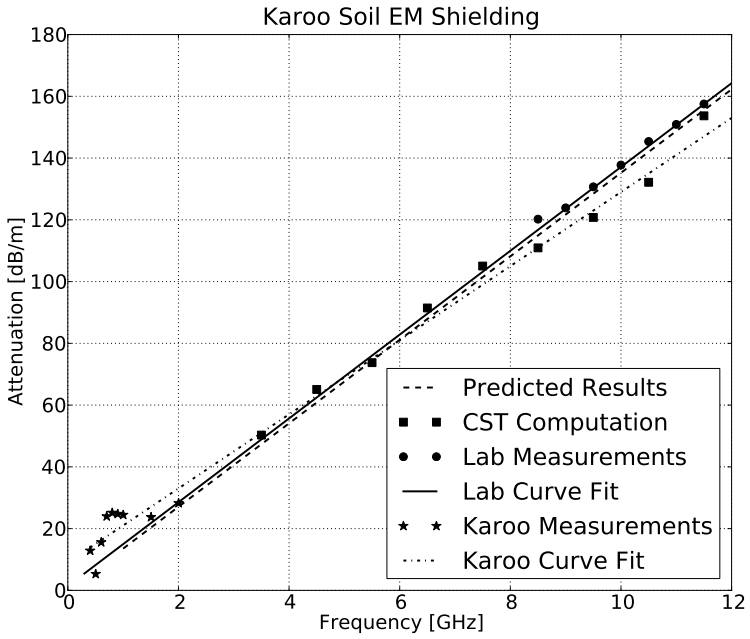

Figure 22: Measured, computed and predicts attenuation values in [dB/m] versus frequency [GHz] for Karoo soil

It is important to remember that the complex permittivity values were only ex-

tracted for the S-band (2.6 to 3.95 GHz) and X-band (8.2 to 12.4 GHz) frequency ranges. These were found to be similar and it was assumed that the real and imaginary permittivity values are constant over the interested frequency range. Good correlation between the predicted and laboratory measured and computed values were obtained. The slight difference in the Karoo site measurements can be due to a number of reasons. One important difference between the site and laboratory measurements is the fact that you have an "infinite" soil/ground plane on-site as apposed to a small finite soil sample in the laboratory. The small sample can cause end scattering field effects of the transmitted signal. The small sample holders also do not have space for larger rocks and stones that is more than likely distributed in layers under the soil surface. It is clear from the results that a signal attenuation between 15 and 150 dB can be expected in the frequency range between 500 MHz and 12 GHz.

It is important to know the complex permittivity values of the Karoo soil in order to use the most accurate values in computational models of the radio telescope dishes and their lightning protection systems. It also gives an indication of the attenuation levels that can be expected when bunkers containing the correlators, control and other electronic equipment are buried under ground at the site complex. These electronic equipment are usually noisy and can easily saturate the extremely sensitive radio receivers at the core-site. The soil would help attenuate these noise signals, as well as protect the equipment from interference from radiative outside noise like lightning.

References

[1] J. Baker-Jarvis, "Transmission/Reflection and Short-Circuit Line Permittivity Measurements," Electromagnetic Fields Division, Center of Electronics and Electrical Engineering, National Engineering Laboratory, National Institute of Standards and Technology, Tech. Rep., July 1990.

[2] A. M. Nicholson and G. Ross, "Measurements of the intrinsic properties of materials by time domain techniques," *IEEE Trans. Intrum. Meas.*, vol. IM-19, pp. 377–382, November 1970.

[3] W. B. Weir, "Automatic measurement of complex dielectric constant and permeability at microwave frequencies," *Proc. IEEE*, vol. 62, pp. 33–36, January 1974.

[4] T. L. Smith, "Vector Network Analyzer Techniques to Measure WR340 Waveguide Windows," Advanced Photon Source, Argonne National Laboratory, Tech. Rep. LS-296, June 26, 2002.

[5] O. Buyukozturk, T. Yu, and J. A. Ortega, "A methodology for determining complex permittivity of construction materials based on transmission-only coherent, wide-bandwidth free-space measurements," *Cement & Concrete Composites*, vol. 28, pp. 349–359, 2006.

[6] R. K. Challa, D. Kajfez, J. R. Gladden, and A. Z. Elsherbeni, "Permittivity Measurements with a Non-Standard Waveguide by Using TRL Calibration and Fractional Linear Data Fitting," in *Progress In Electromagnetics Research B, Vol. 2, pp. 1-13*, 2008.

[7] [Online]. Available: http://www.cst.com/

[8] A. J. Otto and H. C. Reader, "Initial Investigation into the Electromagnetic Shielding Properties of Karoo Soil - Revision 1," MESA Solutions, Tech. Rep., June 2010.

[9] T. W. Miller, B. Borchers, J. M. H. Hendrickx, S. Hong, L. W. Dekker, and C. J. Ritsema, "Effects of Soil Physical Properties on GPR for Landmine Detection," in *Fith International Symposium on Technology and the Mine Problem*, 2002.

[10] M. Riahi and A. Tavangar, "Prognosis of the Effect of Soil Characteristics on the Performance of Landmine Detection in Ground-Penetrating Radar System - A Case Study," in *The 2nd International Conference on Technical Inspection and NDT (TINDT2008)*, October 2008.

Appendices

A S-Parameters

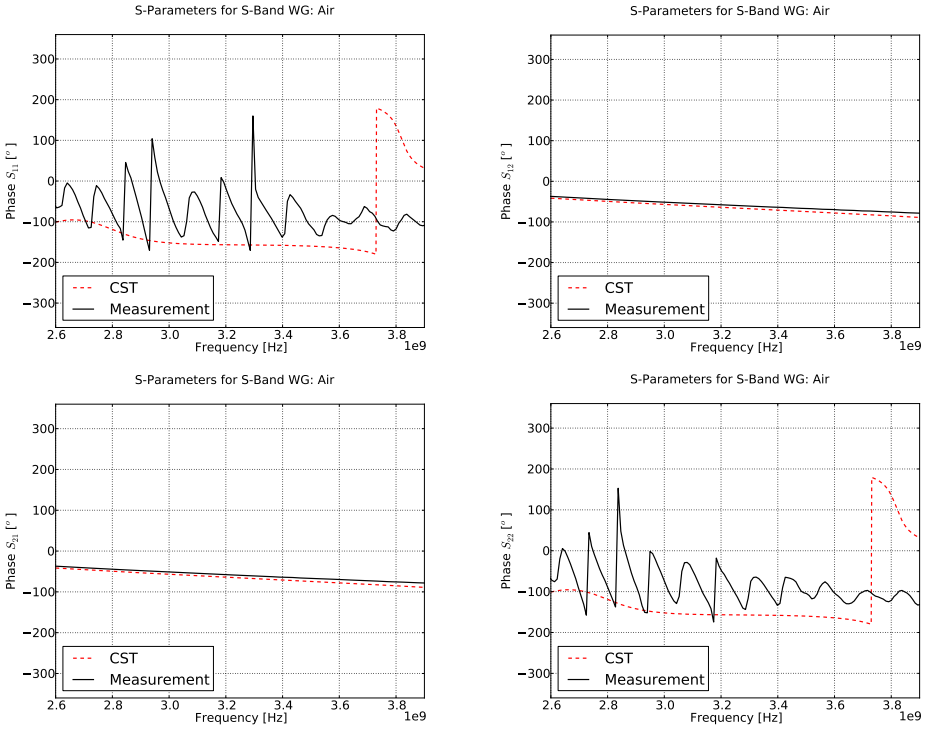

Figure 23: S-Parameters of air sample measured with S-band waveguide (Phase)

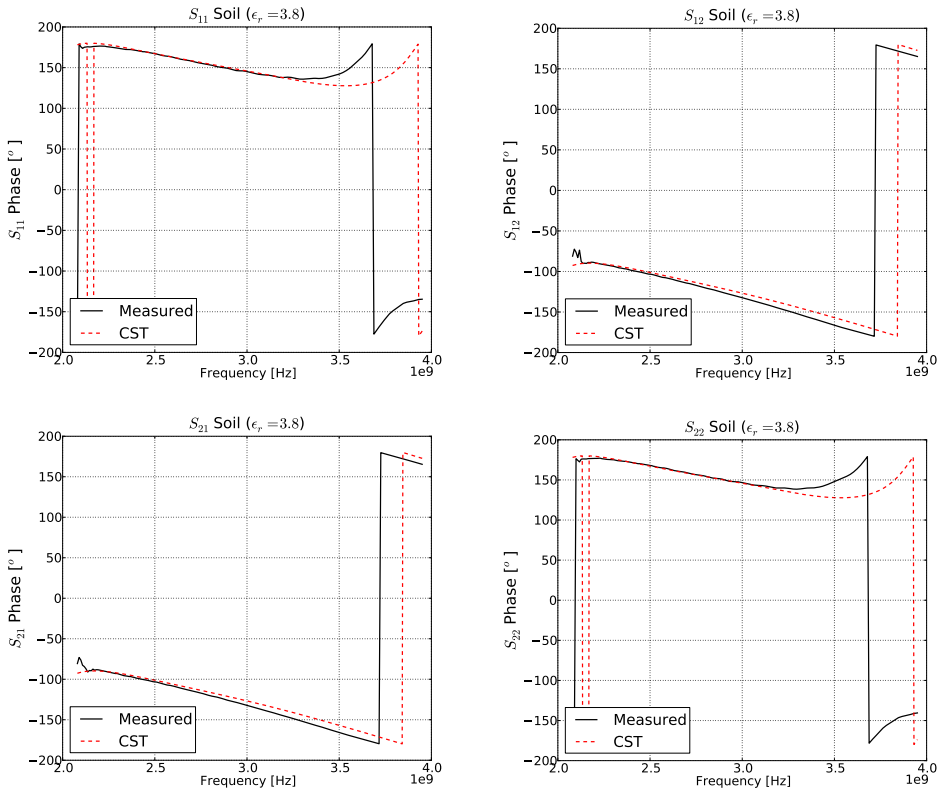

Figure 24: S-Parameters of Karoo soil sample measured with S-band waveguide (Phase)

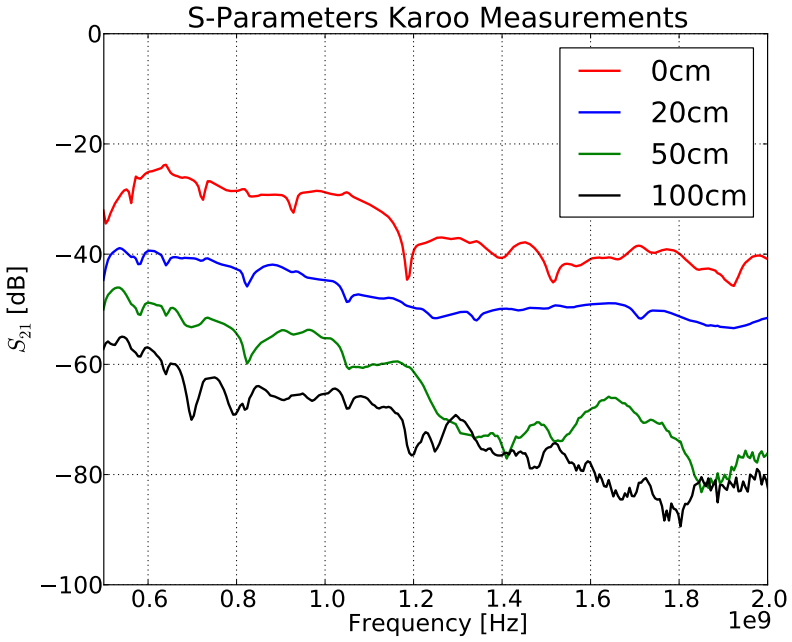

Figure 25: Measured S_{21} for exposed coaxial cable at various depths at Losberg site complex

B Complex Permittivity: Teflon

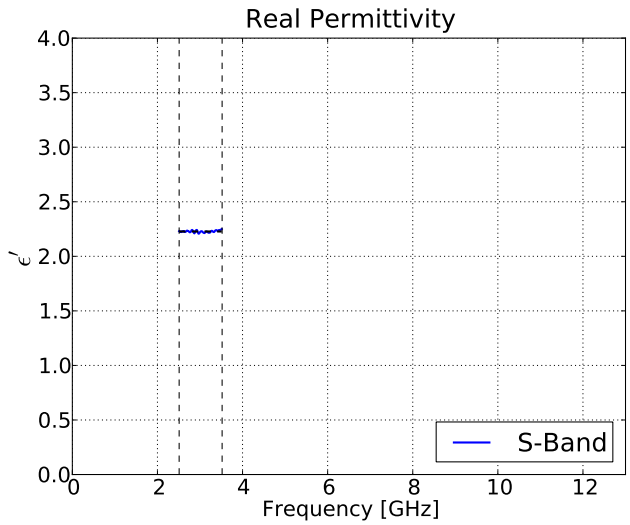

Figure 26: Extracted real value of the complex permittivity of teflon using the BJ method in S-band

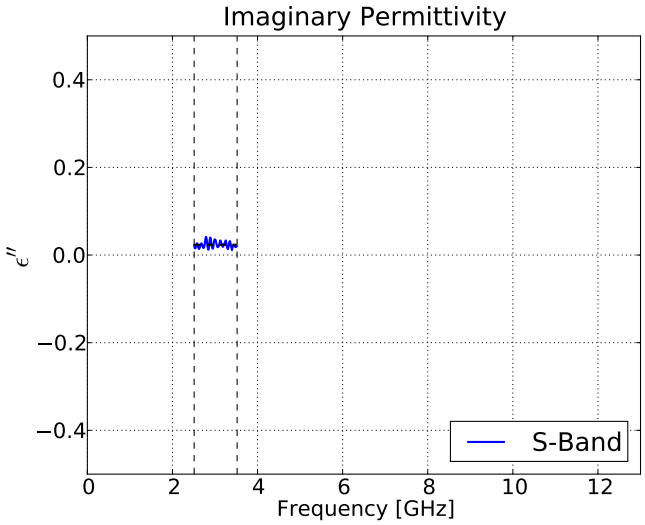

Figure 27: Extracted imaginary value of the complex permittivity of teflon using the BJ method in S-band